J. Anat. (2005) **207**, pp299–312

Intralamellar relationships within the collagenous architecture of the annulus fibrosus imaged in its fully hydrated state

Celina A. Pezowicz,[1] Peter A. Robertson[2] and Neil D. Broom[1]

[1]*Biomaterials Laboratory, Department of Chemical and Materials Engineering, University of Auckland, New Zealand*
[2]*Department of Orthopaedic Surgery, Auckland Hospital, New Zealand*

Abstract

The anisotropic, inhomogeneous, multiply collagenous architecture of the annulus reflects the complex pattern of mainly tensile stresses developed in this region of the disc during normal function. Structural and mechanical responses of fully hydrated in-plane sections taken from within single lamellae of the outer annulus of healthy bovine caudal discs have been investigated using a micromechanical technique in combination with simultaneous high-resolution differential interference contrast optical imaging. Responses both along and across (i.e. transverse to) the primary direction of the mono-array of collagen fibres were studied. Stretching along the alignment direction revealed a biomechanical response consistent with the behaviour of an array whose overall strength is governed primarily by the strength of embedding of the fibres in the vertebral endplates, rather than from interfibre cohesion along their length. The mono-aligned array, even when lacerated, is highly resistant to any further tearing across the alignment direction. Although not visible in the relaxed mono-arrays, transverse stretching revealed a highly complex set of interconnecting structures embodying hierarchical relationships not previously revealed. It is suggested that these structures might play an important role in the containment under pressure of the nuclear contents. The dramatic differences in rupture behaviour observed along vs. across the primary fibre direction are consistent with the known clinical consequences arising from varying degrees of annular wall damage, and might also explain various types of disc herniation. The lamellar architecture of the healthy disc revealed by this investigation provides an important reference framework for exploring structural changes associated with disc trauma and degeneration.

Key words differential interference contrast optical microscopy; disc intralamella structure; hydrated state; interconnecting relationships; micromechanical response; rupture behaviour.

Introduction

The structure of the intervertebral disc (IVD) is both complex and inhomogeneous. In its normal functional state the disc consists of a heavily hydrated gel-like nucleus, which is constrained hydrostatically by the disc wall or annulus. This annulus has a characteristic cross-ply structure consisting of a series of concentric lamellae each containing parallel arrays of collagen bundles aligned oblique to the spine axis and alternating from left to right between successive lamellae (Hirsch & Schajowicz, 1953). Integration of the IVD with its adjoining vertebra is via the cartilaginous endplates (see reviews by Humzah & Soames, 1988; Adams et al. 2002, chapter 8).

When a compressive load is applied to the disc the annular wall experiences both compressive stresses as well as a more complex pattern of in-plane wall stresses generated both by bending and by radial bulging due to the hydrostatic pressure developed in the nucleus. These stresses generated in the annulus are ultimately carried by the arrays of collagen fibres contained within its laminate structure.

Correspondence
Dr Neil Broom, Department of Chemical and Materials Engineering, University of Auckland, Private Bag 92019, Auckland, New Zealand.
E: nd.broom@auckland.ac.nz

Accepted for publication *18 July 2005*

With most uncalcified connective tissues with a primary load-bearing function the associated deformations or strains can be large even under normal physiological loading. The strains developed in the disc wall associated with compressive bending and radial bulging are achieved by large-scale reversible changes in the collagenous architecture both within and between the concentric lamellae. Any major degradation of the interconnecting relationships governing both intra- and interlamellar deformations will lead to a reduction in annular wall strength and a decreased resistance to bulging. This, in turn, will lead to increased radial distension with the potential for eventual prolapse.

Previous investigators have used a variety of mechanical and microscopical techniques applied to isolated portions of the annulus with the aim of elucidating its biomechanical properties. The tensile properties of the annulus as a function of orientation, region, age and degeneration have been extensively investigated (e.g. Galante, 1967; Wu & Yao, 1976; Adams & Green, 1993; Green et al. 1993; Skaggs et al. 1994; Acaroglu et al. 1995; Ebara et al. 1996; Fujita et al. 1997; Elliott & Setton, 2001). Bruehlmann et al. (2004a) used confocal microscopy in combination with biaxial loading to investigate intercellular strains in the outer annulus, the fluorescently labelled nuclei providing the means of tracking strains.

The structure of the annulus has been examined both at the light microscopic level and at the ultrastructural level. For example, Cassidy et al. (1989) examined formalin-fixed histological sections with polarized light, bright-field and Nomarski differential interference contrast (DIC) light microscopy to investigate annular characteristics including lamellar thickness, interlamellar angles, collagen fibre morphology and collagen crimp angle.

Marchand & Ahmed (1990) used a 'dry' peeling method to remove successive annular layers from human lumbar discs. They employed low-resolution stereomicroscopy to investigate laminate configuration and in particular the mechanisms of laminate interruption. The collagen fibril architecture of the annulus has been investigated by Inoue & Takeda (1975) and Inoue (1981), and both histological and immunohistochemical and ultrastructural techniques have been used to examine the much less discussed elastin content of the annulus and nucleus (Buckwalter et al. 1976; Johnson et al. 1982; Yu et al. 2002).

However, a major challenge for disc researchers is to find effective ways of visualizing those structural relationships governing both the large strain and the strength characteristics of the annulus. This requires that the wall be observed under load in its functional state and at a level of resolution able to image the annular structures responding in their 'live' state. [By 'live' we mean maintaining the tissue in its fully hydrated, functional state.]

Unfortunately, with currently available imaging techniques it is experimentally difficult to load the intact hydrated disc while simultaneously viewing its annulus at levels of resolution that are sufficiently high to permit direct imaging of its detailed collagenous architecture. Bruehlmann et al. (2004b) employed a novel confocal microscopy technique to investigate the coupling between the matrix fibres and the cells in intact discs subjected to flexion loading. Bruehlmann et al. (2002) also used confocal imaging to study the three-dimensional distribution of cells in the annulus fibrosus. More recently, magnetic resonance imaging (MRI) techniques have been used to image the lamellar structures of the whole disc (Hsu & Setton, 1999; Wright et al. 2004). Drew et al. (2004) combined MRI with simultaneous compression. However, none of these studies has provided any detailed picture of the fine-scale architecture of the annulus.

Standard histological sections can yield valuable insights into the annular architecture of a disc prepared in a given static state, but cannot track directly changes in its fibrous architecture resulting from physiological loading. At best the histological approach, when combined with *in situ* fixation to 'freeze-in' permanently a given undeformed or deformed state, can provide broad comparisons of structural response. However, such techniques do not permit the 'live' tracking of those large, strain-related rearrangements occurring in the fibrous architecture of the annulus in direct response to load and thus can offer only limited insight into the fundamental mechanisms responsible for its structural cohesion.

Another difficulty is that subjecting a whole disc to a defined load, fixing it in this state and then examining portions of annular tissue sectioned from it may still not provide a particularly meaningful picture of how annular wall strength is achieved in the various structural directions. The sheer complexity of the annular architecture would suggest that a certain amount of structural abstraction or 'dissection' is required in order to reveal in more detail those fundamental relationships governing its deformation behaviour and intrinsic strength.

Although all of the studies mentioned above have yielded important insights into annular properties and structure there still remains much to be learnt about the more detailed relationships that bring about integration of the primary load-bearing elements. Such knowledge should, in turn, provide further insights into the influence of mechanical trauma and early degeneration on annular weakening and the related clinical problem of prolapse.

In an attempt to circumvent some of the experimental limitations discussed above we have used Nomarski DIC optical microscopy combined with simultaneous micromechanical manipulation to image directly the structural response to deformation of fully hydrated layers cut from the annular wall and chosen so as to reveal intralamellar collagenous relationships. A major advantage of the Nomarski technique is that it provides a high-resolution 'live' view of the structural elements while the tissue is maintained in its fully hydrated and thus functional state (Broom, 1984, 1986).

Materials and methods

Ox tails were collected fresh from the local abattoir and immediately frozen for storage. Individual motion segments were removed as required from the frozen tails, thawed, dissected to expose the IVD and then blocks of annulus removed as shown in Fig. 1(A). These blocks were then cryo-glued to a metal base, and frozen serial sections 70–90 μm in nominal thickness were cut in the plane of an outer lamella using a freezing sledging microtome (Fig. 1B). The outer lamellae were selected for sectioning for two important reasons. First, the individual lamellae are most distinct in the outer annulus (Marchand & Ahmed, 1990; Tsuji et al. 1993); slicing from these reduced the difficulty of obtaining sections that incorporated an area within a single lamella sufficiently large for micromechanical testing. Secondly, the greater radius of curvature of the outer lamellae made it easier to cut circumferential sections that again contained a sufficient area of mono-aligned collagen structure from a single lamella, although even with this reduced curvature the sectioned plane, before final trimming, inevitably incorporated structure from more than one lamella.

The cut sections were placed in 0.15 M saline under a cover slip on a glass slide and sorted in order to select samples that contained a region of sufficient area and consisting only of a mono-aligned collagen array. This ensured that the structural observations were confined entirely to within a given lamella. The extraneous tissue was trimmed from these selected regions and the remaining mono-aligned area of tissue further trimmed to create a microtensile sample (viewing dimensions of $\approx 1.5 \times 2$ mm) with the fibre bundle direction along or at 90° to the direction of intended stretching. To make for easier gripping small fabric tabs were glued to the sample ends using cyanoacrylate tissue glue (gel type).

Using the calibrated fine focus control of the DIC microscope and carefully focusing between the upper

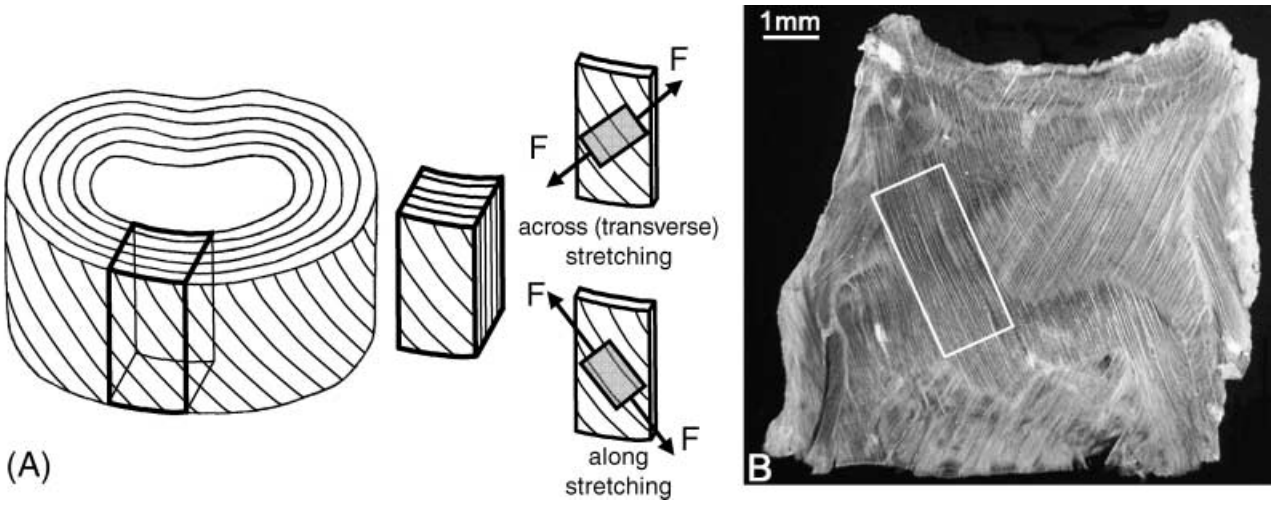

Fig. 1 (A) Schematic diagram showing the procedure for obtaining intralamellar sections suitable for microtensile stretching with an applied force (F) either along or across (transverse) the primary collagen direction while simultaneously viewing 'live' structural response using DIC optical microscopy; (B) a macro view of untrimmed intralamellar section. The mono-aligned test sample cut from this lamellar section is shown in the boxed region.

and lower surfaces the sample thickness was determined at three locations in the midspan region and these values averaged. Vernier callipers were used to obtain the in-plane sample dimensions for nominal stress and strain determination.

The prepared sample was placed in a microtensile device, which mounted directly onto the rotating stage of a DIC optical microscope. Importantly, this device incorporated a system which permitted controlled stretching of the sample within the space between two parallel optical glass surfaces while bathed in physiological saline. In addition, the microtensile device incorporated both load and displacement sensors, thus providing a correlation between structural response, applied stress and degree of stretch. Continuous stress/strain curves were obtained using a tensile displacement rate of 0.4 mm min^{-1}. Tensile strains were expressed as strain ratios λ (i.e. stretched length/original length). Because all samples required the addition of fabric tabs to facilitate their gripping in the microtensometer, all strain values must be considered as nominal due to the slight stretching of these tabs.

The relatively low rate of tensile extension employed in the tests permitted simultaneous photographic recording of the progressively loaded structure up to medium levels of magnification. In order to capture more accurately the progression of structural response, all high-resolution structural observations were recorded as still images under conditions in which the tensile displacement was applied manually and discontinuously. By combining the results from both experiments it was possible to correlate satisfactorily the structural and mechanical data.

Approximately nine annular blocks from three caudal discs taken proximally from two healthy ox tails were prepared and sectioned. For high-resolution structural studies approximately ten sections were examined while being stretched discontinuously along the collagen alignment direction and 26 similarly stretched across this direction (i.e. transversely). A further 14 sections were examined structurally while being subjected to continuous tensile loading, eight in the collagen alignment direction and six in the transverse direction.

Results

A typical lamellar section is shown in its untrimmed form in Fig. 1(B). The smaller mono-aligned boxed region was cut from this untrimmed section and tested.

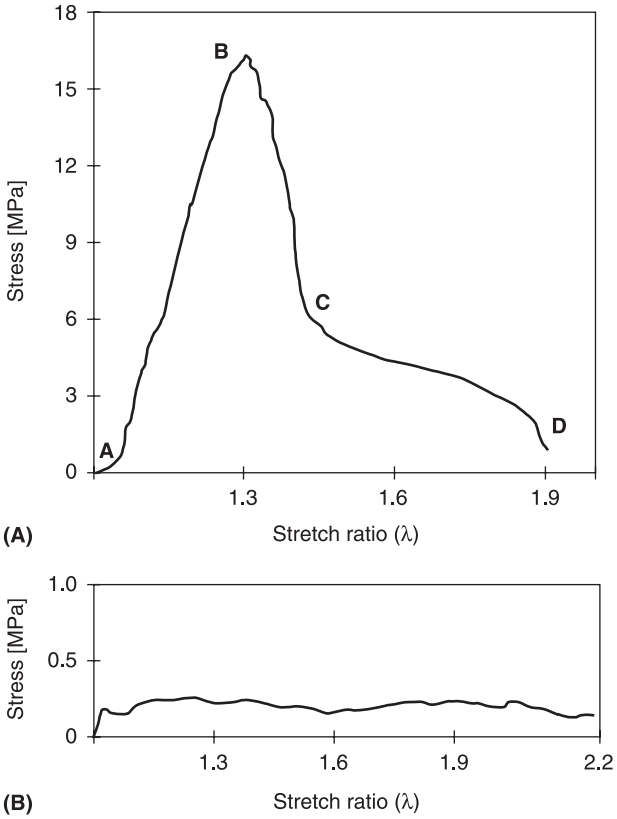

Fig. 2 Tensile stress/strain responses obtained from mono-aligned samples stretched (A) along the collagen alignment direction, and (B) transverse to the collagen alignment direction.

Mechanical and structural response with tensile stretching along fibre alignment direction

Figure 2(A) is a typical stress/strain response obtained from a sample stretched in the aligned direction using continuous loading. The initial phase of the curve (A to B) identifies the region of response in which the in-phase crimp is progressively straightened, leading to isolated bundle sliding within the otherwise intact array at point B (see Fig. 3A,B). This sliding occurred along the entire length of the sample, indicating that these isolated bundles had detached or pulled out from one or other of the glued ends, and signalled the commencement of the rupture process. The rapidly declining stress region B to C corresponds to the progressive increase in bundle sliding and separation throughout much of the array (Fig. 4A,B). Point C also marks the commencement of the reduced stress region of behaviour resulting from the large-scale separation of fibre bundles (Fig. 4C), this separation ending finally at D. Note in particular the return of the collagen crimp as the fibre bundles unload following their detachment

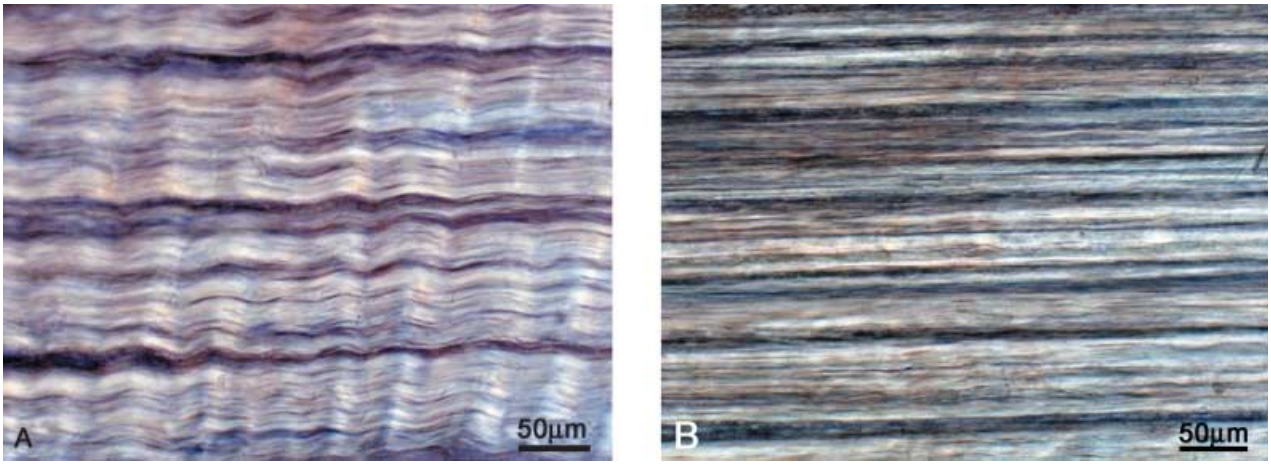

Fig. 3 Reversible stretching of an intralamellar sample along the collagen fibre direction showing the straightening of the in-phase crimp.

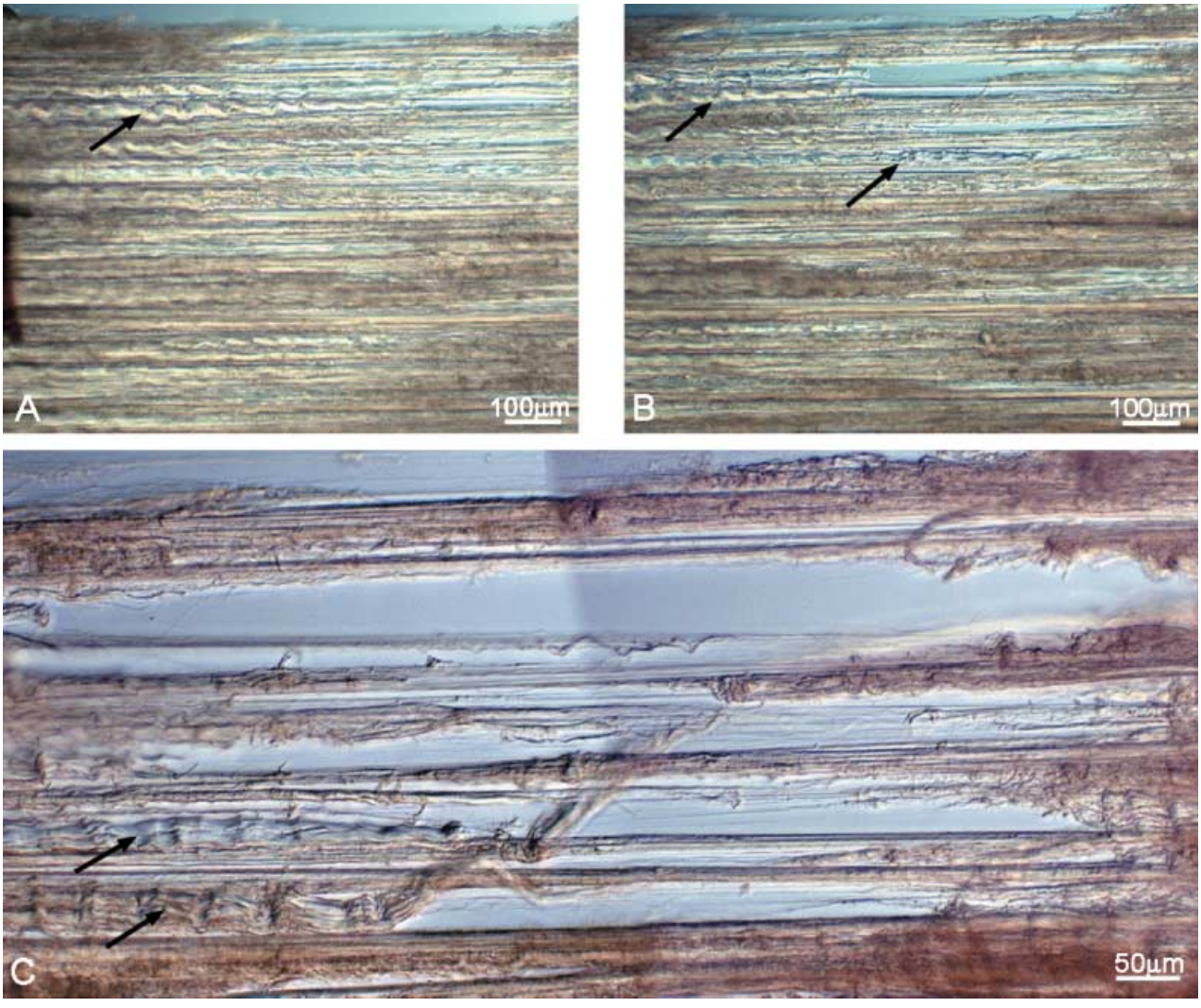

Fig. 4 (A,B) Progressive pullout and separation of the fibre bundles; (C) magnified view revealing extensive fibre sliding and separation.

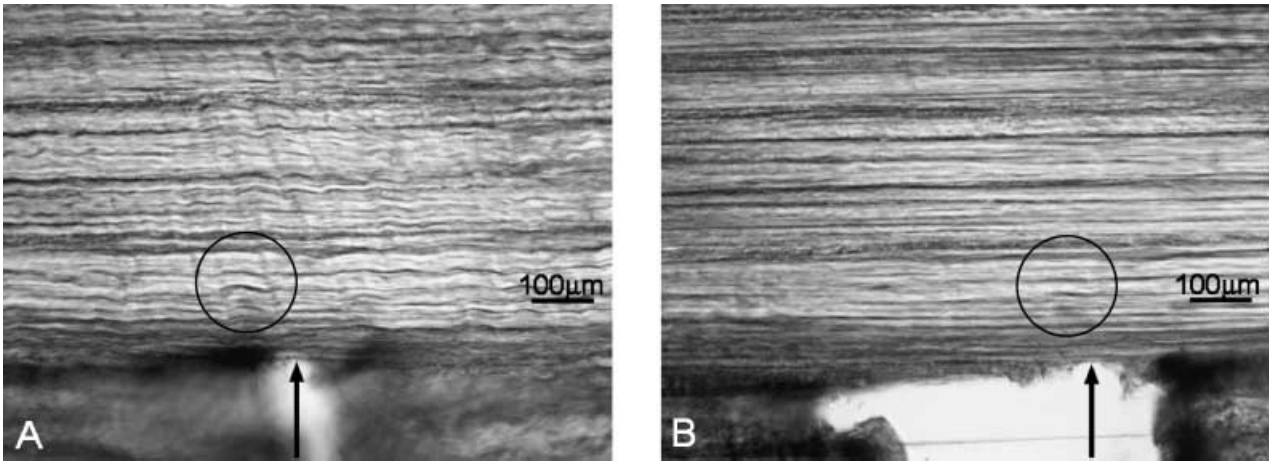

Fig. 5 Mono-aligned array containing an artificial transverse notch and loaded in tension up to the point of generalized rupture elsewhere in the sample. The original notch site is indicated by an arrow. The circled region in each image indicates the same site in the unloaded and loaded states. Note that there is no detectable propagation of this notch across the primary array.

from the grips (see regions marked with arrows in Fig. 4B,C). Failure of the mono array under this mode of loading was thus gradual rather than precipitous.

All eight mono-aligned samples that were tested in continuous loading exhibited the same general mechanical and structural response shown in Figs 2(A), 3 and 4. Importantly, although the stress maximum (point B in Fig. 2A) was highly variable (mean = 16.4 MPa, SD = 8 MPa), the stress defining the onset of large-scale bundle separation across the full width of the array (point C in Fig. 2A) showed much less variability (mean = 5.5 MPa, SD = 1.8 MPa). This same mode of progressive failure was observed even when a small transverse cut or notch was made on one side of the collagenous array so as to sever locally its continuity (Fig. 5A,B). No localized propagation of this notch across the array could be induced before progressive rupture developed elsewhere within the array, as described in Fig. 4(A–C).

Mechanical and structural response with tensile stretching across fibre alignment direction

Figure 2(B) shows a continuous stress/strain response typical of the lamellar sections subjected to stretching in a direction transverse to the collagen alignment direction. Viewed at a relatively low magnification the initially parallel bundles of fibres progressively 'separated' from the main body of the array (see sites marked V_1 and V_2 in Fig. 6) while undergoing extensive lateral rearrangement at a nearly constant level of stress. Six samples were tested in this mode with an average initial peak stress of 0.15 MPa (SD = 0.06 MPa).

Interrupted manual stretching in combination with higher resolution imaging provided a more detailed picture of the structural response of these transversely stretched arrays. The mono-aligned array in Fig. 7(A) is shown progressively stretched in Fig. 7(B–D). The aligned bundles of fibres begin to separate in isolated regions of the array exposing a network of residual collagenous interconnections that crossed obliquely from both left (L) to right (R) and R to L of the now divided array (e.g. see site marked W in Fig. 7B,C). With increased stretching these same clefts opened even further, accompanied by extensive skewing of the still intact fibre bundles (Fig. 7D).

The stretched state in Fig. 7(D) is shown in Fig. 7(E) at a higher magnification and reveals in greater detail the complexity of this interconnecting or bridging structure. Note, for example, in Fig. 7(E) the larger number of relatively bulky bundles that pass downwards from L to R as compared with the fewer number passing downwards from R to L. Secondly, the more bulky L–R bundles are further subconnected by a much finer structure with a downwards R–L orientation (Fig. 7E). Two other examples of this two-way or dual cross-over of the primary bundles are shown in Fig. 8(A,B) and represented one of the two common forms of transverse interconnectivity within the primary array identified in this study.

The second identifiable type of transverse interconnectivity involved only a single direction of cross-over of the primary bundles, which we term mono-interconnectivity. Figure 9(A) clearly shows bulky primary bundles that have split off from the originally intact array now crossing

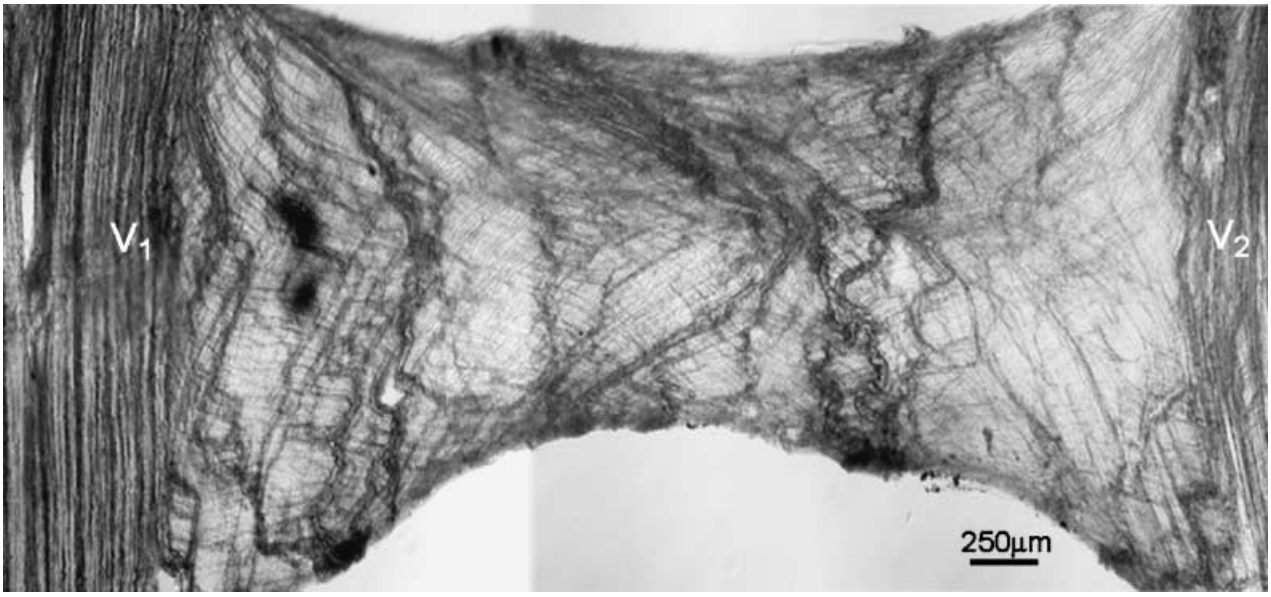

Fig. 6 Low-magnification view of the progressive transverse separation of the original mono-aligned arrays (see sites V_1, V_2). Note the extensive skewing of the fibre bundles.

the opening cleft downwards only from L to R (see site marked X_1). A similar region of mono-interconnectivity but from R to L can be seen at X_2 in the same image. A secondary level of bridging structure is also generated by further stretching and splitting of the primary bridging bundles. This is seen to a minor extent in Fig. 9(A) at X_3 and in Fig. 9(B) at Y, but also more visibly in Fig. 9(C) (see Z_1). A further subdivision of these sub-bundles can be seen in Fig. 9(D) (see Z_2).

Discussion

This study has shown that it is possible to image, at a high level of optical resolution, the structural response of fully hydrated sections of disc lamellae that are being simultaneously stretched along or across the primary fibre alignment direction.

As with other mono-aligned collagenous arrays exhibiting an in-phase crimp morphology (e.g. Broom, 1978; Cassidy et al. 1989), reversible tensile loading of our sections along the primary alignment direction resulted in progressive straightening and restoration of this crimp. With increased loading the section eventually ruptured, but not from a focal tear propagating across the entire array, but rather via a far more diffuse failure mechanism. As fibres in one localized region of high stress pulled out, the increased local strain transferred the applied load to fibres in other regions, which in turn pulled out. This repeating cycle, involving a sequential recruitment of the load-bearing elements, led to a characteristically multisite, generalized pattern of progressive rupture (Fig. 4).

Failure in such specialized structures is thus gradual rather than catastrophic, and the mechanism involved confers on them an enhanced degree of toughness even in the presence of some pre-existing region of weakness. [In the present context 'rupture strength' refers to the stress (or force per unit area) required to break or create two separate surfaces of the original material. 'Toughness' refers to the work or energy required to achieve this separation. It is thus a force $\times$ stretch (or displacement) term.] This was seen in the behaviour of samples that had been prenotched (Fig. 5) and in which it was impossible to propagate failure from these local sites of weakness. Instead, diffuse rupture occurred involving many regions of the sample, as illustrated in Fig. 4.

The stresses required to initiate rupture in the samples stretched along the alignment direction will be substantially lower than would be required had we been able to retain *in vivo* anchorage. While the glued fabric tabs provided a degree of longitudinal anchorage for the trimmed array, this cannot compare with the strength of mechanical fixation in the intact motion segment. *In vivo* the fibre bundles in each lamella are embedded either in the cartilaginous endplate or, as with the outermost fibres, they insert directly in the vertebral bone (Adams et al. 2002, p. 15). Our peak

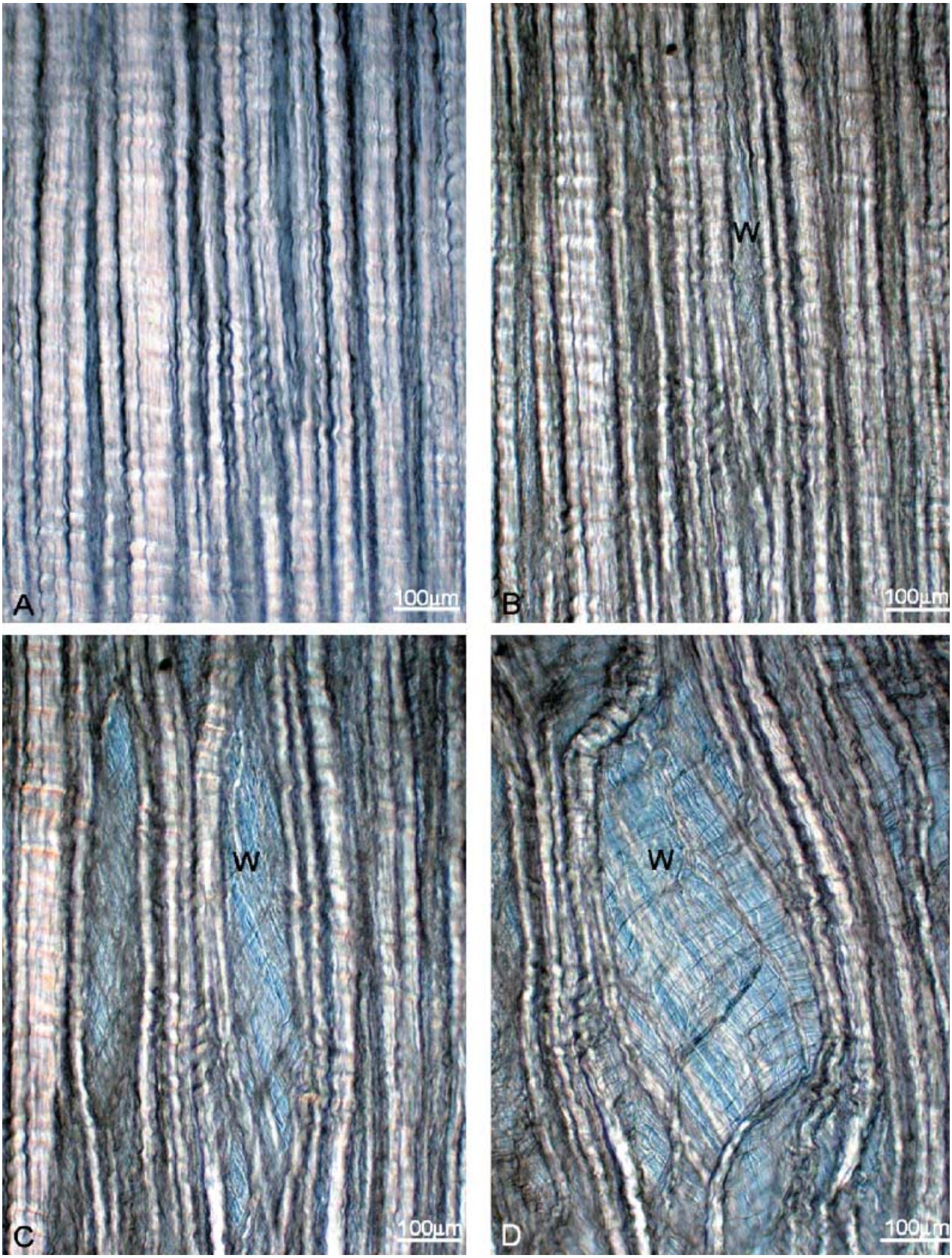

Fig. 7 (A–D) The mono-aligned array in A is subjected to progressive transverse stretching in B to D to reveal an extensive interconnecting structure in the cleft region marked W. (E) The cleft region W shown in D but at higher resolution.

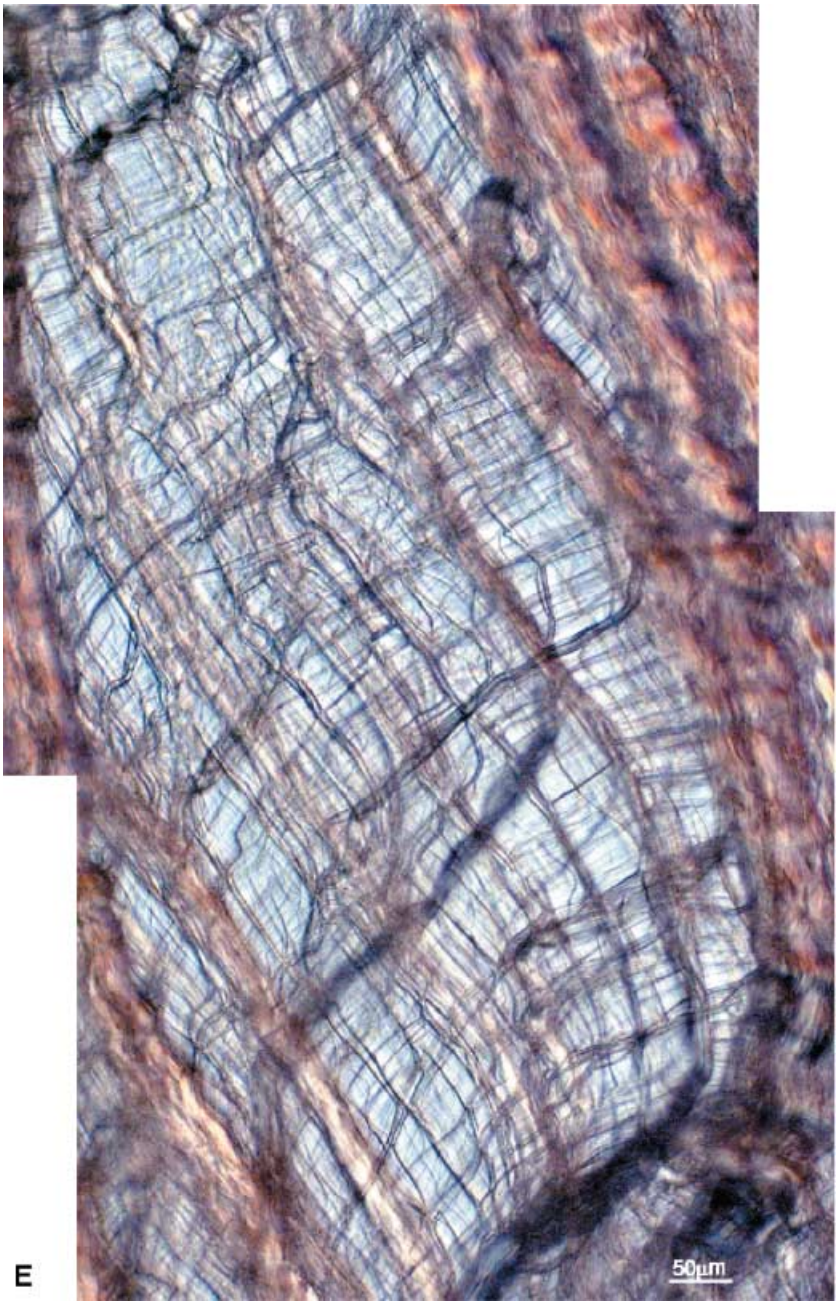

Fig. 7 *Continued*

stress values obtained from stretching along the fibre alignment direction will be both variable because of the lack of consistency in the glueing process, and lower than any value to be expected from samples where the *in vivo* anchorage is retained (Green et al. 1993).

Observing the early stages of rupture while loading samples separately in the two orthogonal directions has helped clarify a fundamental question: to what extent does the tensile strength of the annulus depend on fibres coursing uninterrupted from bone to bone (or endplate to endplate) vs. reliance on some form of interfibre cohesion that would enable shorter, discontinuous fibres to still achieve the required degree of reinforcement? This latter mechanism has been suggested by other disc investigators who have invoked classical chopped-fibre-reinforced composite ideas (Hukins & Aspden, 1985; Adams & Green, 1993; Green et al. 1993). With loading in the alignment direction the peak stress always coincided both with the sudden onset of sliding of isolated bundles over their entire visible length between the gripped ends and with a rapid

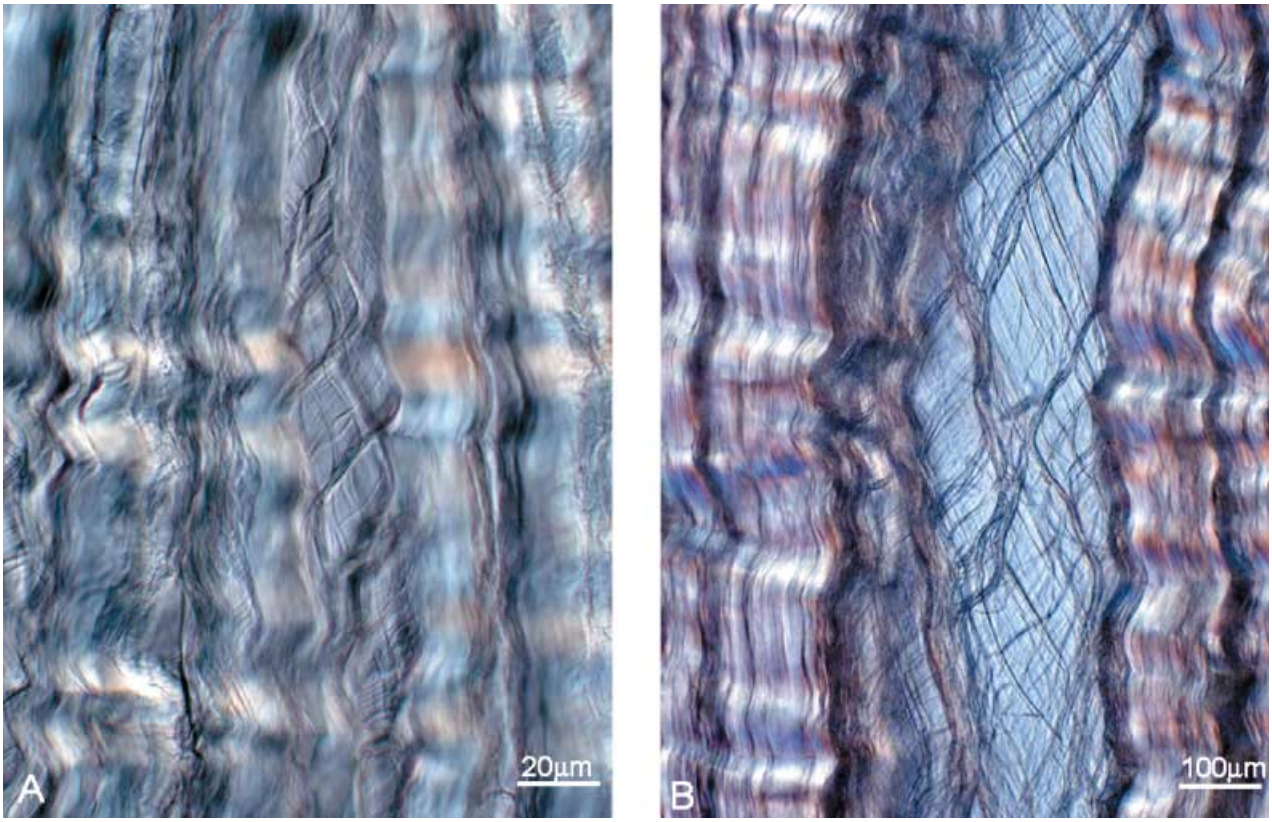

Fig. 8 Examples of dual cross-over of collagen bundles in the cleft region revealed by transverse stretching.

reduction in stress (see B to C in Fig. 2A). This suggests a fibre anchorage mode of failure rather than simply a breakdown in the cohesion between discontinuous fibre bundles. This does not mean that there is no interfibre cohesion. Rather, its role in contributing to intra-annular tensile strength and stiffness is probably minor. This interpretation is further confirmed by the low levels of stress required to achieve progressive separation of the fibre bundles once large-scale pullout of the array has occurred (see Fig. 4C and region C–D in Fig. 2A).

The transverse stretching experiments also support the fibre anchorage interpretation. The low levels of stress required to separate the initially parallel fibre bundles and to re-orientate them extensively (Figs 2B and 6) are inconsistent with a model of annular stiffness and strength derived from relatively strong interfibre cohesive forces. In this type of tissue system, the primary functional requirements are low stress flexibility and high ultimate strength and stiffness. If annular strength is derived from discontinuous fibres bonded to each other through some mediating matrix, e.g. the proteoglycans as suggested by Adams & Green (1993), then we are required to attribute a substantial fraction of the strength of the mono-aligned array (see region A to B in Fig. 2A) as much to the bonding component as to the fibres themselves. The difficulty with this interpretation is that unless the strength of bonding between the discontinuous fibres is of a sufficient magnitude there will be insufficient transfer of load from one discontinuous fibre to another and interfibre sliding will occur. The consequences of having a very low level of fibre/matrix interaction will be a highly flexible composite system but possessing low ultimate strength. In such a system increasing the strength of bonding between the discontinuous fibres and matrix will facilitate the transmission of load across the discontinuous array, but at the expense of flexibility. [This latter mechanical outcome, i.e. high strength and stiffness, is what is aimed for in most high-performance engineering composites.]

Conversely, a crimped aligned array of fibres continuous from one anchored end to the other is entirely consistent with the experimental observations reported in this study. Such a system provides the required mix of functional properties as follows: (a) high flexibility

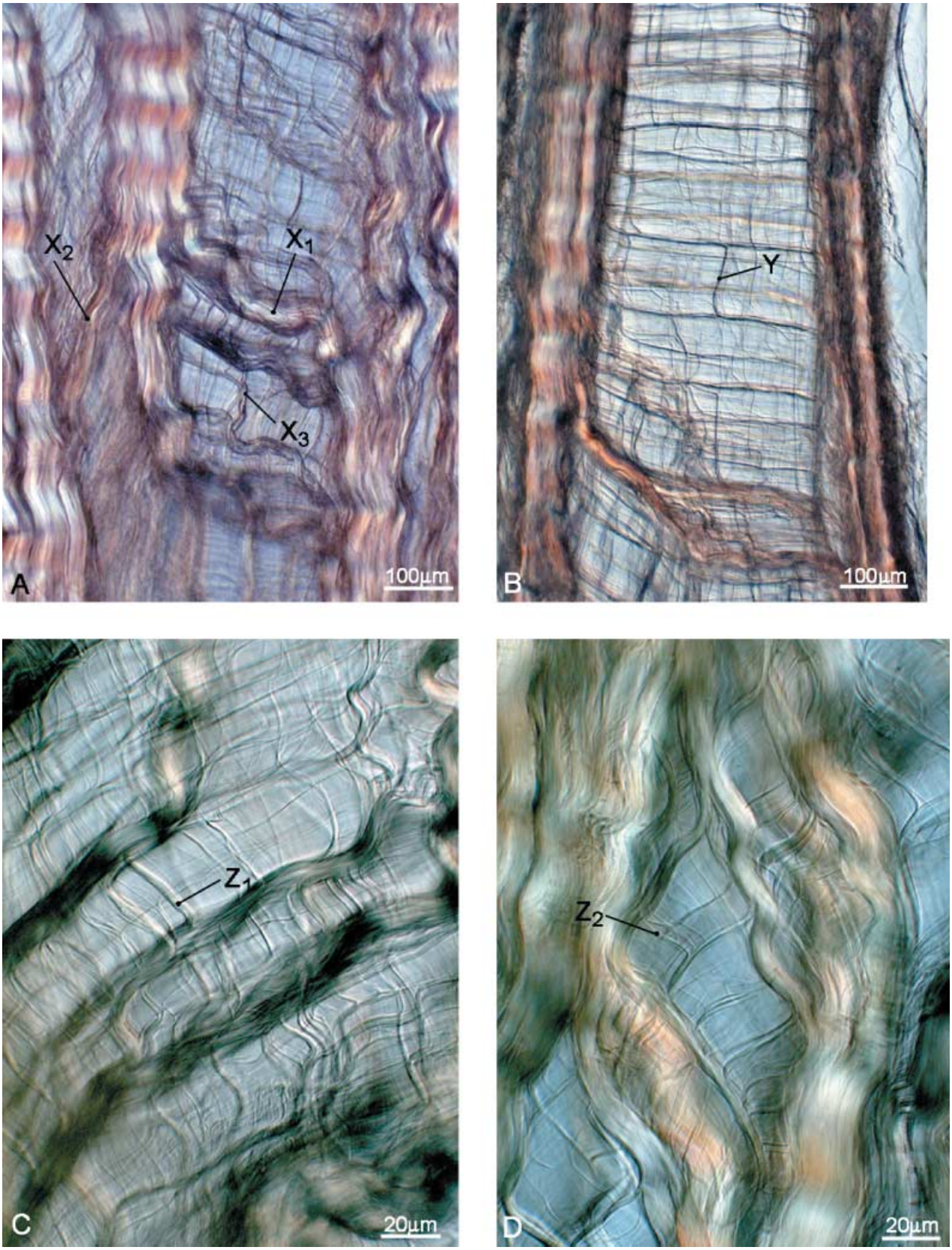

Fig. 9 Examples of interconnectivity involving a single direction of cross-over, but also involving splitting and subsplitting of these bridging elements (see text).

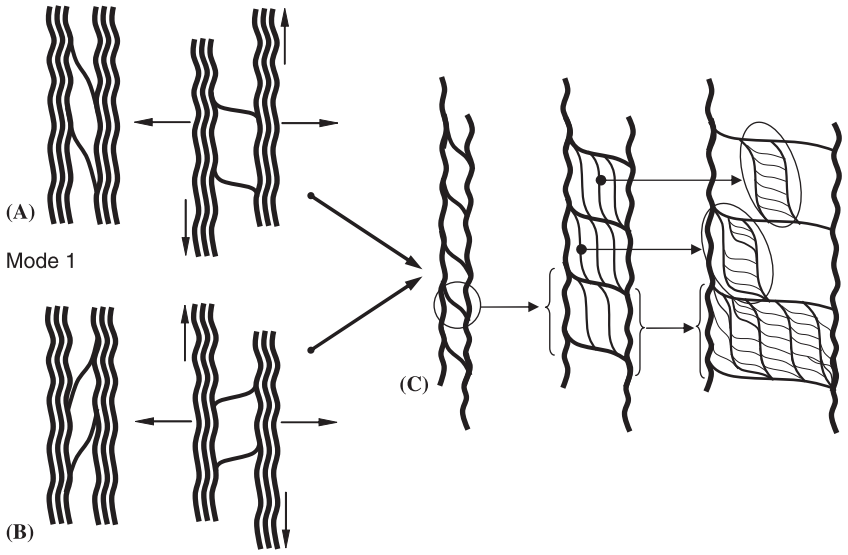

Fig. 10 Schematic diagram of interconnectivities involving mono cross-over of collagen fibres with subsequent splitting and subsplitting.

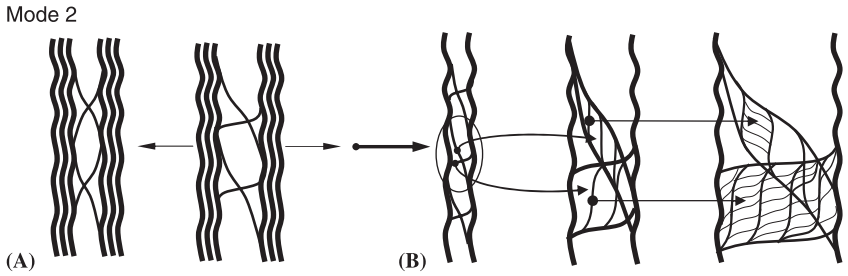

Fig. 11 Schematic diagram showing more complex dual cross-over of interconnecting elements and subsequent splitting and subsplitting.

at lower stresses, (b) rapid stiffening as the crimp straightens reversibly, (c) high rupture strength due to the secure anchorage of the fibres in the vertebral bone/endplate and (d) high toughness due to the large amount of mechanical work (or energy) needed to pull out the anchored fibres. Further evidence that the strength of the array is due primarily to the end-anchorage of the fibres rather than derived from significant fibre/matrix interactions is seen from the ease with which the collagen crimp is reversibly straightened (see region A in Fig. 2A). A high level of interaction would effectively 'straight-jacket' the fibres, making them resistant to uncrimping. The reverse is what we observe experimentally.

The transverse stretching experiments (Figs 6–9) clearly demonstrated that the mono-aligned arrays within a lamella are highly integrated across the primary direction of alignment. Superficially the mode 1 form of interconnectivity (L–R or R–L) is the least complex in that it involves only a single direction of cross-over (Fig. 9). Yet this mode still involves the sub/subsplitting of the mono-bridging elements, as depicted schematically in Fig. 10(A–C). The more complex interconnecting mode 2 structures formed by the dual cross-over of bundles and their subsequent sub/subsplitting (Figs 7 and 8) is shown schematically in Fig. 11(A,B). Interestingly, the large amount of skewing in many regions of the originally parallel array occurring under transverse stretching is readily accounted for by these different modes of interconnection. The mode 1 type of cross-over shown in Fig. 10(A,B) is highly skewable. Conversely, in regions where the mode 2 dual cross-over operates the degree of skewing will tend to be more restricted (Fig. 11).

Given that the lamellae derive their primary tensile strength from the aligned fibre bundles anchored into the vertebral endplates, what might be the role of this extensive interconnecting structure, which becomes microscopically visible only when the annular layers are subjected to transverse stretching? The radial bulging associated with direct compression of the disc will inevitably result in a degree of separation of the

mono-aligned bundles in the lamellae. The hierarchical sub/subsplitting meshwork structure might then act as a captive meshwork immobilizing the proteoglycan aggregates while still allowing the outflow of water.

From a clinical perspective, the resistence to further propagation of a partial transverse laceration of lamellae fibres (see Fig. 5) is consistent with the observation that needle passage through the annulus during discography does not result in radiological or clinical deterioration over time (Kahanovitz et al. 1986; Johnson, 1989). Conversely, a more major annular division over multiple layers of lamellae is known to initiate disc degeneration (Osti et al. 1990). One presumes that this latter animal model involves a far greater level of destruction of longitudinal fibres in multiple lamellae compared with that inflicted by discography needle penetration.

The ease of transverse separation of the in-plane fibres (Fig. 2B) is consistent with the clinical observation of disc herniation involving only nuclear and annular material, which presumably occurs through a similar transverse separation of fibres (Moore et al. 1996). A second common form of herniation involves additional protrusion/extrusion of cartilaginous endplate (Harada & Nakahara, 1989; Brock et al. 1992). This latter type might reflect failure at the annulus/endplate junction, the study of which is a logical progression of the present work.

Another aspect of potential clinical relevence concerns the reported observation of a genetic predisposition to disc degeneration (Simmons et al. 1996; Varlotta et al. 1991; Battie et al. 1995). The mechanism responsible for this is unclear but biomechanical variations secondary to differing collagen types (Eyre et al. 2002) might provide an explanation for variable levels of fibre interconnectivity and subsequent vulnerability to failure under load.

Finally, the detailed structural picture arising from this 'live' tissue study provides a potentially valuable reference framework for investigating mechanisms of annular weakening associated both with disc trauma and with degeneration.

Acknowledgements

This research was supported by a research grant generously provided by the Auckland Medical Research Foundation. C.A.P. is grateful for the leave granted to her by Professor R. Bedzinski of the Wroclaw University of Technology, Poland.

References

Acaroglu ER, Iatridis JC, Setton LA, Foster RJ, Mow VC, Weidenbaum M (1995) Degeneration and aging affect the tensile behavior of human lumbar anulus fibrosus. *Spine* **20**, 2690–2701.

Adams MA, Green TP (1993) Tensile properties of the annulus fibrosis. I. The contribution of fibre–matrix interactions to tensile stiffness and strength. *Eur Spine J* **2**, 203–208.

Adams M, Bogduk N, Burton K, Dolan P (2002) *The Biomechanics of Back Pain*. Churchill Livingstone, London.

Battie MC, Videman T, Gibbons LE, Fisher LD, Manninen H, Gill K (1995) 1995 Volvo Award in clinical sciences. Determinants of lumbar disc degeneration. A study relating lifetime exposures and magnetic resonance imaging findings in identical twins. *Spine* **20**, 2601–2612.

Brock M, Patt S, Mayer HM (1992) The form and structure of the extruded disc. *Spine* **17**, 1457–1461.

Broom ND (1978) Simultaneous morphological and stress–strain studies of the fibrous components in wet heart valve leaflet tissue. *Connective Tissue Res* **6**, 37–50.

Broom ND (1984) Further insights into the structural principles governing the function of articular cartilage. *J Anat* **139**, 275–294.

Broom ND (1986) The collagenous architecture of articular cartilage – a synthesis of ultrastructure and mechanical function. *J Rheumatol* **13**, 142–152.

Bruehlmann SB, Rattner JB, Matyas JR, Duncan NA (2002) Regional variations in the cellular matrix of the annulus fibrosus of the intervertebral disc. *J Anat* **201**, 159–171.

Bruehlmann SB, Hulme PA, Duncan NA (2004a) In situ intercellular mechanics of the bovine outer annulus fibrosus subjected to biaxial strains. *J Biomech* **37**, 223–231.

Bruehlmann SB, Matyas JR, Duncan NA (2004b) Collagen fibril sliding governs cell mechanics in the annulus fibrosus. *Spine* **29**, 2612–2620.

Buckwalter JA, Cooper RR, Maynard JA (1976) Elastic fibres in human intervertebral discs. *J Bone Joint Surg* **58-A**, 73–76.

Cassidy JJ, Hiltner A, Baer E (1989) Hierarchical structure of the intervertebral disc. *Connective Tissue Res* **23**, 75–88.

Drew SC, Silva P, Crozier S, Pearcy MJ (2004) A diffusion and T_2 relaxation MRI study of the ovine lumbar intervertebral disc under compression *in vitro*. *Phys Med Biol* **49**, 3585–3592.

Ebara S, Iatridis JC, Setton LA, Foster RJ, Mow VC, Weidenbaum M (1996) Tensile properties of nondegenerate human annulus fibrosis. *Spine* **21**, 452–461.

Elliott DM, Setton LA (2001) Anisotropic and inhomogeneous tensile behaviour of the human annulus fibrosus: experimental measurements and material model predictions. *J Biomech Eng* **123**, 256–263.

Eyre DR, Matsui Y, Wu JJ (2002) Collagen polymorphisms of the intervertebral disc. *Biochem Soc Trans* **30**, 844–848.

Fujita Y, Duncan NE, Lotz JC (1997) Radial tensile properties of the lumbar annulus fibrosis are site and degeneration dependent. *J Orthop Res* **15**, 814–819.

Galante JO (1967) Tensile properties of the human lumbar annulus fibrosus. *Acta Orthop Scand Suppl* **100**, 1–91.

Green TP, Adams MA, Dolan P (1993) Tensile properties of the annulus fibrosis. II. Ultimate tensile strength and fatigue life. *Eur Spine J* **2**, 209–214.

Harada Y, Nakahara S (1989) A pathologic study of lumbar disc herniation in the elderly. *Spine* **14**, 1020–1024.

Hirsch C, Schajowicz F (1953) Studies on structural changes in the lumbar annulus fibrosus. *Acta Orthop Scand* **22**, 184–231.

Hsu EW, Setton LA (1999) Diffusion tensor microscopy of the intervertebral disc annulus fibrosus. *Mag Reson Med* **41**, 992–999.

Hukins DWL, Aspden RM (1985) Composition and properties of connective tissues. *TIBS* **10**, 260–264.

Humzah MD, Soames RW (1988) Human intervertebral disc: structure and function. *Anat Rec* **220**, 337–356.

Inoue H, Takeda T (1975) Three-dimensional observation of collagen framework of lumbar intervertebral discs. *Acta Orthop Scand* **46**, 949–956.

Inoue H (1981) Three-dimensional architecture of lumbar intervertebral discs. *Spine* **6**, 139–146.

Johnson EF, Chetty K, Moore IM, Stewart A, Jones W (1982) The distribution and arrangement of elastic fibres in the intervertebral disc of the adult human. *J Anat* **135**, 301–309.

Johnson RG (1989) Does discography injure normal discs? An analysis of repeat discograms. *Spine* **14**, 424–426.

Kahanovitz N, Arnoczky SP, Sissons HA, Steiner GC, Schwarez P (1986) The effect of discography on the canine intervertebral disc. *Spine* **11**, 26–27.

Marchand F, Ahmed AM (1990) Investigation of the laminate structure of lumbar disc annulus fibrosus. *Spine* **15**, 402–410.

Moore RJ, Vernon-Roberts B, Fraser RD, Osti OL, Schembri M (1996) The origin and fate of herniated lumbar intervertebral disc tissue. *Spine* **21**, 2149–2155.

Osti OL, Vernon-Roberts B, Fraser RD (1990) 1990 Volvo Award in experimental studies. Anulus tears and intervertebral disc degeneration. An experimental study using an animal model. *Spine* **15**, 762–767.

Simmons ED Jr, Guntupalli M, Kowalski JM, Braun F, Seidel T (1996) Familial predisposition for degenerative disc disease. A case-control study. *Spine* **21**, 1527–1529.

Skaggs DL, Weidenbaum M, Iatridis JC, Ratcliffe A, Mow VC (1994) Regional variation in tensile properties and biochemical composition of the human lumbar annulus fibrosus. *Spine* **19**, 1310–1319.

Tsuji H, Hirano N, Ohshima H, Ishihara H, Terahata N, Motoe T (1993) Structural variation of the anterior and posterior annulus fibrosis in the development of human lumbar intervertebral discs: a risk factor for intervertebral disc rupture. *Spine* **18**, 204–210.

Varlotta GP, Brown MD, Kelsey JL, Golden AL (1991) Familial predisposition for herniation of a lumbar disc in patients who are less than twenty-one years old. *Bone Joint Surg Am* **73**, 124–128.

Wright AC, Elliott DM, Johannessen W, Vresilovic EJ, Wehrli FW (2004) MRI measurement of collagen orientation in whole intervertebral discs. *Proc Intl Soc Mag Reson Med* **11**, 1519.

Wu H-C, Yao R-F (1976) Mechanical behaviour of the human annulus fibrosus. *J Biomech* **9**, 1–7.

Yu J, Peter C, Roberts S, Urban JPG (2002) Elastic fibre organisation in the intervertebral discs of the bovine tail. *J Anat* **201**, 465–475.